

Low-lying structures in the Gamow-Teller strength functions for the double-beta-decaying nuclei ^{76}Ge , ^{82}Se , ^{128}Te , and ^{130}Te

R. Madey, B. S. Flanders,* B. D. Anderson, A. R. Baldwin, and J. W. Watson
Department of Physics, Kent State University, Kent, Ohio 44242

Sam M. Austin

Department of Physics and Astronomy and Cyclotron Laboratory, Michigan State University, East Lansing, Michigan 48824

C. C. Foster

Indiana University Cyclotron Facility, Bloomington, Indiana 47405

H. V. Klapdor and K. Grotz

Max-Planck-Institut für Kernphysik, Heidelberg, Federal Republic of Germany

(Received 31 March 1989)

Excitation-energy distributions of transition strength to 1^+ states excited via the (p,n) reaction at 134.4 MeV on targets of ^{76}Ge , ^{82}Se , ^{128}Te , and ^{130}Te were measured for excitation energies up to 25 MeV. Structures observed in the neutron spectra with forward-peaked ($\Delta L=0$) angular distributions were identified as 1^+ states, except for the isobaric analog transitions. The total 1^+ strength in these reactions was extracted by normalizing the intensity in the 1^+ peaks to the Fermi transition strength observed in the isobaric analog state. The Gamow-Teller strength observed in 1^+ peaks above a fitted polynomial background is typically 55% of the sum rule obtained by assuming that the strength of β^+ transitions is negligible. The portion of this strength found at excitation energies less than that of the Gamow-Teller giant resonance varied from 15% for ^{128}Te to 38% for ^{76}Ge . Experimental results are compared with predictions of a shell model that includes a pairing force and a long-range Gamow-Teller force in both parent and daughter nuclei. A comparison of the strength functions of the tellurium isotopes is made; this comparison is relevant in determining whether double-beta decay without neutrino emission (0ν decay) is observed in these isotopes.

I. INTRODUCTION

The ability to survey experimentally the dominant portion of Gamow-Teller (GT) strength makes the (p,n) reaction a valuable complement to weak-interaction decays. At bombarding energies above about 100 MeV, the nature of the operator mediating (p,n) transitions is such that the neutron spectrum at 0° from a (p,n) reaction on a 0^+ target nucleus is dominated by transitions to 1^+ states. The quantum numbers for a 0^+ to 1^+ transition are $\Delta J=1$, $\Delta L=0$, and $\Delta S=1$, the same as those for an allowed ($\Delta L=0$) Gamow-Teller ($\Delta S=1$) transition in beta decay. Because the (p,n) and GT operators are so similar, the neutron-energy spectrum at 0° (i.e., at low momentum transfer) is expected to be proportional to the GT strength function. This proportionality is found experimentally to be quite accurate.

Studies on many 0^+ target nuclei reveal that the transition strength to the Gamow-Teller giant resonance (GTGR) is quenched in the sense that the GTGR peak contains less GT strength than expected on the basis of a general model-independent sum rule for allowed ($\Delta L=0$) GT ($\Delta S=1$) beta decay.^{1,2} In this paper, we present an investigation of the GT strength distribution in the reactions $^{76}\text{Ge}(p,n)^{76}\text{As}$, $^{82}\text{Se}(p,n)^{82}\text{Br}$, $^{128}\text{Te}(p,n)^{128}\text{I}$, and $^{130}\text{Te}(p,n)^{130}\text{I}$ at 134.4 MeV. With detection techniques

described previously,³ we achieved energy resolutions of typically 350 keV (FWHM) and observed structures in the neutron time-of-flight spectra at 0.3 deg from below the GTGR up to an excitation energy of ~ 25 MeV in the residual nucleus. All structures with forward-peaked ($\Delta L=0$) angular distributions, except for the transition to the isobaric-analog state (IAS), were identified as 1^+ transitions. The GT strength in each of these structures was extracted from the cross sections of the 1^+ peaks above a fitted polynomial background.⁴ These cross sections were normalized to the Fermi transition strength, which is concentrated in the IAS transition, and which nearly exhausts the sum rule for Fermi transitions. The percentage of the GT sum rule extracted this way is about 57% when the β^+ transitions that connect states of a spin-orbit pair are blocked by the Pauli principle.

The four nuclei studied here have energetically allowed double-beta-decay channels available. Double-beta ($\beta\beta$) decay is a two-step second-order weak process, where the intermediate single-beta-decay state is energetically inaccessible and is passed through as a virtual intermediate state. Experimental information, as well as theoretical understanding, especially of the low-lying part of the GT distribution in the above reactions, is needed to improve the predictions for $\beta\beta$ -decay rates. Measurements of the low-lying GT strength functions for $\beta\beta$ -decay nuclei can

be used to provide constraints on calculations of the matrix elements involved in the first step of the $\beta\beta$ -decay processes. Such an understanding is required if limits on the mass of the electron neutrino are to be established by comparing calculated lifetimes for $\beta\beta$ decay with measured lifetimes.⁵⁻⁸

The case of the tellurium isotopes is particularly interesting, in the sense that the measured ratio of half-lives for the $\beta\beta$ decay of these nuclei can be used to determine whether $\beta\beta$ decay without the emission of neutrinos (0ν decay) is observed in these nuclei. (The normal process involves the emission of two electrons and two antineutrinos and is denoted here as 2ν decay.) The 0ν process is of exceptional interest because its observation implies non-conservation of leptons, and its intensity can be used to place limits on the mass of a Majorana neutrino or on the presence of right-handed weak currents. The lifetime ratio analysis requires that the ratio of the matrix elements be known; therefore, we analyzed the data in order to obtain with accuracy the ratio of the Gamow-Teller strength for ^{128}Te and ^{130}Te , and to provide an estimate of the difference of the matrix elements in these neighboring nuclei.

II. EXPERIMENTAL PROCEDURE

The measurements were carried out at the Indiana University Cyclotron Facility with the beam-slinger system.⁹ The beam slinger is capable of deflecting the incident proton beam through an angle of up to 26 deg. Neutrons were detected in mean-timed¹⁰ neutron detectors³ located at 0, 24, and 45 deg to the undeflected proton beam. The data reported in this paper came from the 0 deg detector station with a flight path from the target to the detector array of 85.8 ± 0.2 m. The detector array consisted of three NE-102 plastic scintillators, each 1.02-m long by 0.508-m high by 10.2-cm thick, with a total frontal area of 1.55 m². Protons from the target were rejected by an anticoincidence detector in front of the array. Cosmic rays were rejected by anticoincidence detectors on top and at the front of the array. The details of the electronics and the data acquisition system are similar to those described previously.¹¹

Unpolarized protons with an energy of 134.4 MeV were incident on targets of ^{76}Ge , ^{82}Se , ^{128}Te , and ^{130}Te . The thickness of each target and the estimated uncertainty in the thickness are listed in the second column of

Table I. The ^{130}Te target was found to be contaminated with oxygen from exposure to air. Transitions to the $2^-/3^-$ (0.42/0.72 MeV), 1^+ (4.65 MeV), and $1^+/4^-$ (6.23/6.37 MeV) states in ^{16}F are observed in the spectrum from ^{130}Te (see Fig. 8). The ^{76}Ge target was supported with a 400- $\mu\text{g}/\text{cm}^2$ polyethylene $(\text{CH})_n$ foil; accordingly, the spectrum from this target reveals the ^{12}N ground-state peak from the $^{12}\text{C}(p,n)$ reaction. This peak is seen also for the three other targets (see Figs. 5-8).

Neutron energies were measured by the time-of-flight (TOF) technique with an energy resolution (FWHM) of about 350 keV for 130-MeV neutrons. Time-of-flight spectra were measured at average laboratory angles of 0.3, 4.0, and 8.4 deg. Spectra from each detector in the array were recorded at many pulse-height thresholds ranging from 25 to 90 MeVee (MeV of equivalent-electron energy). Calibration of the pulse-height response of each of the detectors was performed with a ^{232}Th γ source (which emits a 2.6-MeV γ ray) and a calibrated fast amplifier. During the experiment the calibration was checked periodically with this source and found to be stable to within 10%. Absolute cross sections obtained for several thresholds (from 40 to 70 MeVee) were the same within statistics. The cross sections were extracted with efficiencies calculated with the Monte Carlo code of Cecil *et al.*¹² These efficiencies were checked by comparing various (p,n) and (p,p') analog transitions and were found to be accurate to better than $\pm 10\%$.¹³⁻¹⁵ Efficiencies obtained from the measurement¹⁵ of $^7\text{Li}(p,n)$ activation cross sections are consistent with these (Monte Carlo) calculated efficiencies.

The energy resolution achieved with each target for a pulse-height threshold of 50 MeVee is listed in Table I. Quoted numbers are the FWHM of the lowest-lying isolated peak in the neutron excitation-energy spectra: the IAS in ^{76}As and in ^{130}I , the 1^+ state at 78 keV in ^{82}Br , and the 1^+ ground state in ^{128}I . The neutron energy associated with each of these peaks is listed in Table I. The energy resolution of 338 keV (FWHM) for 132.3-MeV neutrons from the $^{128}\text{Te}(p,n)$ ^{128}I (g.s.) reaction corresponds to a time dispersion of 622 ps. We estimate the contributions to the overall time dispersion to be (i) the intrinsic time dispersion of the neutron detectors (~ 300 ps), (ii) a nominal beam-energy spread of about 0.1% (~ 270 ps), (iii) the finite target thickness (~ 300 ps), (iv) the neutron transit time across the effective thickness of the detector (~ 430 ps), and (v) the dispersion in the tim-

TABLE I. Energy resolutions achieved with (p,n) reactions at 134.4 MeV on targets of ^{76}Ge , ^{82}Se , ^{128}Te , and ^{130}Te .

Target	Thickness		Neutron energy E (MeV)	Energy resolution (FWHM)		
	t (mg/cm ²)	Δt		ΔE (keV)	$\Delta E/E$ (%)	Final state
^{76}Ge	33.7	1.7	124.4	383	0.31	IAS
$^{82}\text{Se}^a$	43.4	2.1	133.5	370	0.26	$1^+, E_x = 78$ keV
^{128}Te	48.2	2.4	132.3	338	0.26	$1^+, \text{g.s.}$
^{130}Te	45.1	2.3	120.7	326	0.27	IAS

^aBecause of a crack in the ^{82}Se target, the effective thickness traversed by the beam is probably 30-40% smaller.

ing signal obtained from the cyclotron radio frequency (i.e., the beam-burst width) (~ 350 ps). The contributions from the thickness of the target and the thickness of the detector are rectangular distributions. Because the standard deviation of a rectangular distribution is equal to the width divided by $(12)^{1/2}$, the associated full width at half maximum is 205 ps for the contribution from the target thickness and 293 ps for the contribution from the detector thickness. The quadrature combination of these five contributions yields a resolution of 643 ps, which is close to the observed resolution.

III. DATA REDUCTION

The neutron TOF spectra were converted to neutron-energy spectra by selecting an appropriate reference TOF in each spectrum. The reference point used for each of the four reactions studied here is listed in Table II; in each case, the reference point is a neutron peak that corresponds to the excitation of a state of known energy in the residual nucleus. Shown in panel (a) of Figs. 1–4 are the excitation-energy spectra at 0.3 deg with a 50-MeV pulse-height threshold and without subtraction of any background. The main features of these spectra are (1) a dominant narrow peak resulting from the 0^+ IAS transition, (2) a large broad bump at higher-excitation energy than the IAS from the excitation of the 1^+ Gamow-Teller giant resonance, (3) two or three narrow peaks at very low-excitation energies ($\lesssim \sim 2$ MeV), and (4) one or more broad-structured bumps of varying magnitude in the excitation energy region above 2 MeV and below the IAS.

The computer code ALLFIT (Ref. 16) was used to fit the TOF spectra at 0.3 deg with as many peaks as the structure warranted on top of a polynomial background. The peaks were fitted simultaneously with the background, which was required to account for the so-called “wrap-around” and residual cosmic-ray backgrounds below the ground state as well as the continuum region above ≈ 20 MeV of excitation. The “wrap-around” background arises from slow neutrons from earlier beam bursts. The “wrap-around” background beneath each spectrum is an extrapolation of a straight line through the background below the ground state. This extrapolated straight line is weighted by the energy-dependent neutron detection efficiency. The line shape chosen for the peaks was an asymmetric hyperGaussian of the form

$$(H \exp[(x-p)^\gamma / 2\sigma_\pm^2]),$$

where H is the height, p is the position, σ_+ (σ_-) is the width in the positive (negative) x direction, and γ is the exponent. Because all of the peaks were fitted simultane-

ously, the parameters of the shape were weighted by the strength of the peaks; hence, they were determined largely by the IAS and the GTGR. The widths of the low-lying peaks were varied together because they should be determined largely by instrumental factors. The widths of the other peaks were determined from the minimization of χ^2 ; the number of peaks chosen to fit the broad, unresolved structures was determined subjectively by the observed structures. The TOF spectra with the peak fitting results are shown in Figs. 5–8. The arrows denote peaks with forward-peaked ($\Delta L=0$) angular distributions. The label m above a peak indicates that the angular distribution is a mixture of a $\Delta L=0$ transition with $\Delta L \neq 0$ transitions. A peak was declared to be mixed when its angular distribution deviated clearly from a forward-peaked ($\Delta L=0$) shape. For mixed transitions, the 1^+ strength at 0.3 deg was estimated by fitting the angular distribution with a weighted sum of $\Delta L=0$ and $\Delta L=1$ shapes, which are calculated with a distorted-wave impulse-approximation (DWIA) code.¹⁷ These calculations used the effective interaction of Franey and Love¹⁸ and the optical potentials of Schwandt *et al.*¹⁹

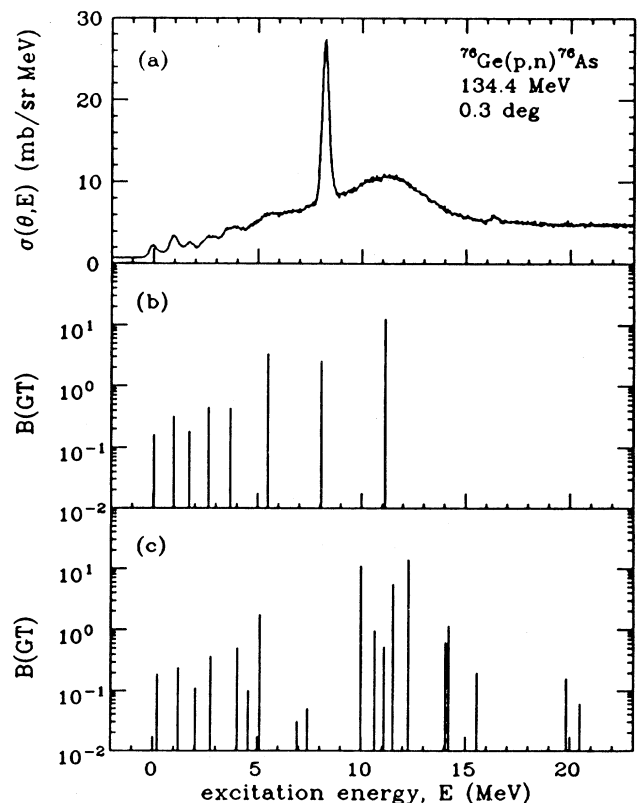


FIG. 1. Gamow-Teller strength distribution for the $^{76}\text{Ge}(p,n)^{76}\text{As}$ reaction. (a) is the excitation-energy spectrum at 0.3 deg and 134.4 MeV. The bars in (b) are values of $B(\text{GT})$ extracted from the spectrum in (a); those in (c) are from a BCS-pairing model calculation.

TABLE II. Reference points for converting neutron time-of-flight spectra to energy spectra.

Reaction	Reference peak
$^{76}\text{Ge}(p,n)^{76}\text{As}$	1^+ doublet at $E_x = 46$ and 87 keV
$^{82}\text{Se}(p,n)^{82}\text{Br}$	1^+ , $E_x = 78$ keV
$^{128}\text{Te}(p,n)^{128}\text{I}$	1^+ , g.s.
$^{130}\text{Te}(p,n)^{130}\text{I}$	2^+ , $E_x = 48$ keV

The fraction of the strength attributed to the $\Delta L=0$ shape was taken to represent 1^+ strength. Most of the strength observed in the peaks at 0.3 deg for each of these targets was associated with the $\Delta L=0$ shape; however, states without $\Delta L=0$ strength were observed in ^{82}Br at $E_x=1.50$ and 2.70 MeV, and in ^{130}I at $E_x=0.08$ and 4.20 MeV. Given an energy resolution of ~ 350 keV and a typical level spacing in the residual nuclei of a few tens of keV, each of the fitted peaks except for the IAS transitions and a few very low-lying transitions correspond most likely to an unresolved group of states. Because the spins and parities are known only for a few states in these residual nuclei, the excitation energies of the peaks were determined solely from the fits to the measured spectra. Excitation energies in the final nucleus are accurate to about 100 keV, in general, and are within 40 keV of published values for the few states with known energies.

After fitting the spectra at 0.3°, the spectra at the other two angles were fitted which as many peaks as the structure in the spectra appeared to warrant. The extracted excitation energies agreed usually within a few tens of keV with those extracted at 0.3 deg; in a few cases where

larger differences were observed, the positions of the peaks were fixed to the values obtained at 0.3 deg. Changes in the number of peaks fitted to a spectrum affects only the distribution of excitation energies of the extracted strength. Because many choices in the number of peaks can reproduce the overall spectral shape, detailed comparisons with the position of the individual extracted peaks should not be made.

Gamow-Teller strength was extracted previously in the $^{26}\text{Mg}(p,n)$ reaction with the same experimental apparatus.²⁰ In that measurement, a quasifree background was calculated in a plane-wave impulse approximation with a modified version of the code written by Wu.²¹ Comparison of the quasifree background with a polynomial background of the type used in the present analysis yielded cross sections which agreed to better than 13% in the region of excitation energy that corresponds to the region of interest here. Quasifree calculations were not performed here because neutron separation energies were unavailable to us for the shells of interest; however, as described in Sec. VI, we estimated the GT strength in the subtracted background.

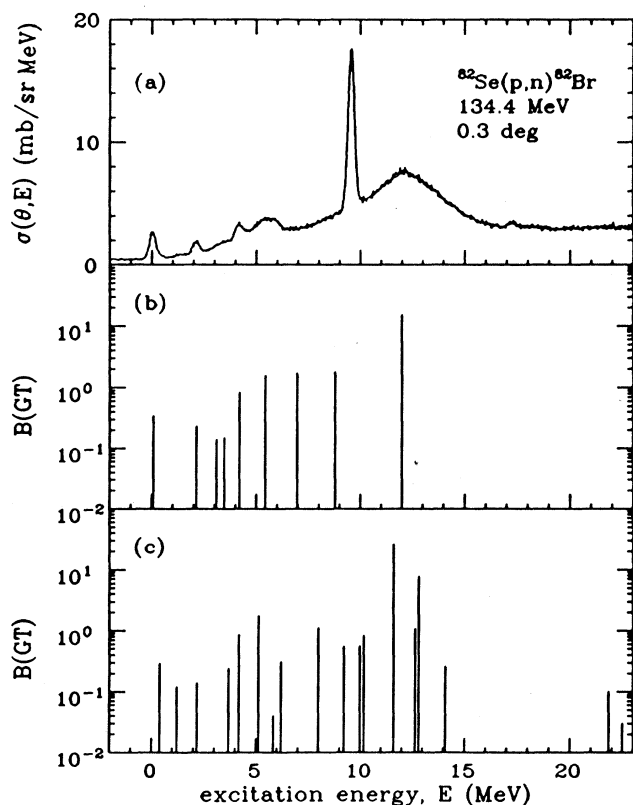


FIG. 2. Gamow-Teller strength distribution for the $^{82}\text{Se}(p,n)^{82}\text{Br}$ reaction. (a) is the excitation-energy spectrum at 0.3 deg and 134.4 MeV. The bars in (b) are values of $B(\text{GT})$ extracted from the spectrum in (a); those in (c) are from a BCS-pairing model calculation. The absolute cross sections are probably too small by 50–60 % because of a crack in the ^{82}Se target.

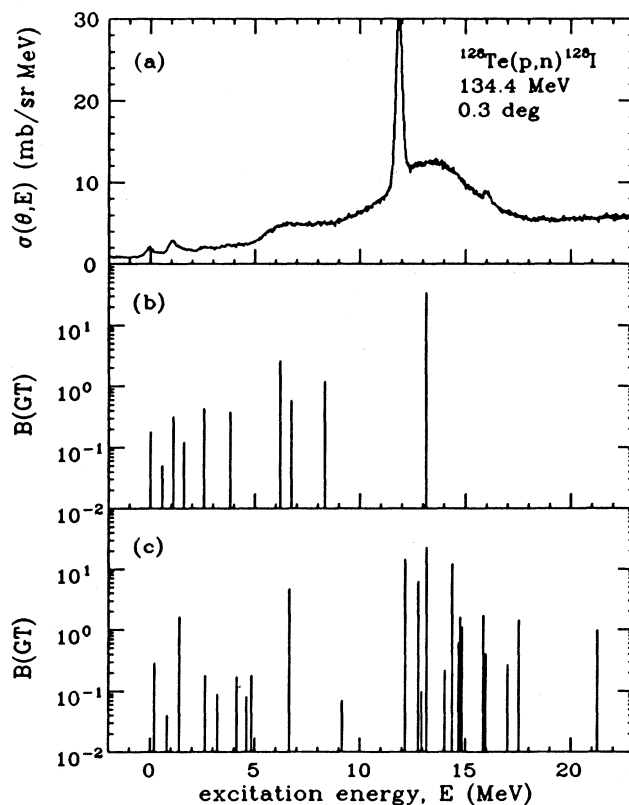


FIG. 3. Gamow-Teller strength distribution for the $^{128}\text{Te}(p,n)^{128}\text{I}$ reaction. (a) is the excitation-energy spectrum at 0.3 deg and 134.4 MeV. The bars in (b) are values of $B(\text{GT})$ extracted from the spectrum in (a); those in (c) are from a BCS-pairing model calculation.

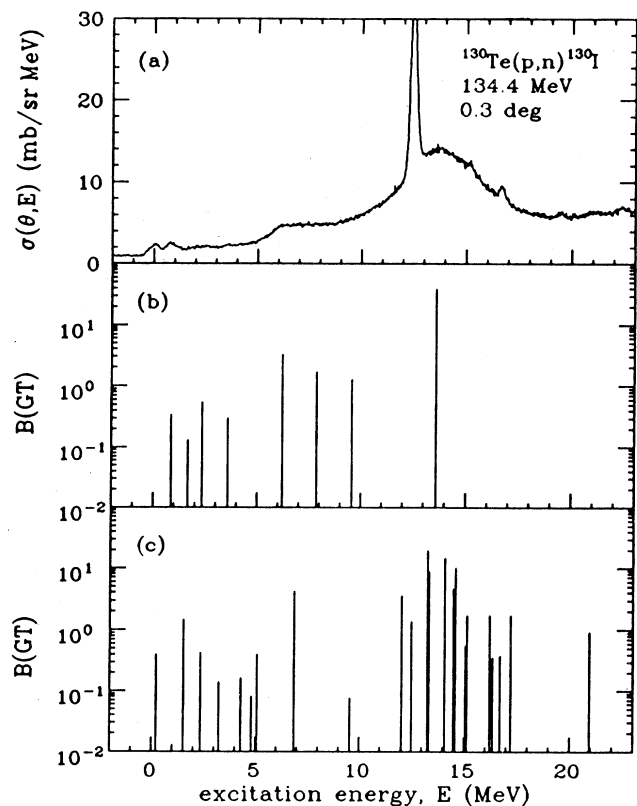


FIG. 4. Gamow-Teller strength distribution for the $^{130}\text{Te}(p,n)^{130}\text{I}$ reaction. (a) is the excitation-energy spectrum at 0.3 deg and 134.4 MeV. The bars in (b) are values of $B(GT)$ extracted from the spectrum in (a); those in (c) are from a BCS-pairing model calculation.

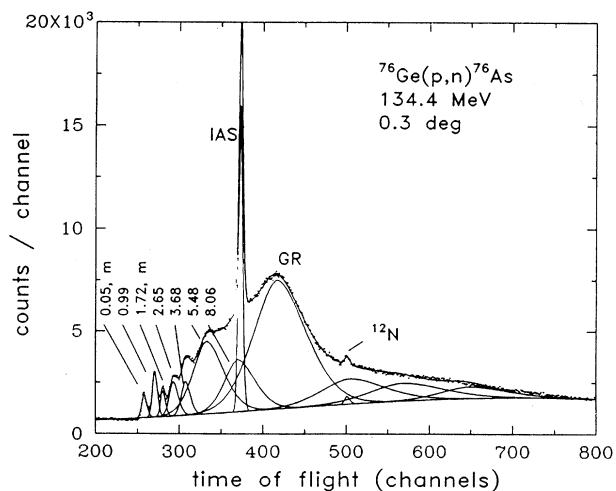


FIG. 5. Neutron time-of-flight spectrum at 0.3 deg from the $^{76}\text{Ge}(p,n)^{76}\text{As}$ reaction at 134.4 MeV. The solid lines show the results of using the code ALLFIT to fit the peaks simultaneously above the polynomial background shown.

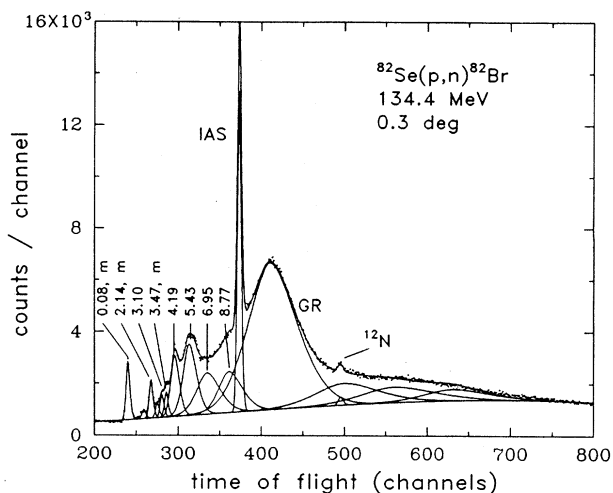


FIG. 6. Neutron time-of-flight spectrum at 0.3 deg from the $^{82}\text{Se}(p,n)^{82}\text{Br}$ reaction at 134.4 MeV. The solid lines show the results of using the code ALLFIT to fit the peaks simultaneously above the polynomial background.

IV. CROSS SECTIONS

We extracted the angular distribution of each peak observed in the spectra at 0.3 deg, identified $\Delta L=0$ strength in the residual nuclei up to 25 MeV, extracted its intensity, and estimated the Gamow-Teller strength for each $\Delta L=0$ transition. The angular distributions of the differential cross sections for the peaks observed in the spectra at 0.3 deg from (p,n) reactions on ^{76}Ge , ^{82}Se , ^{128}Te , and ^{130}Te are listed in Tables III–VI, respectively. The absolute cross sections for these transitions were extracted from the known target thickness, beam-current

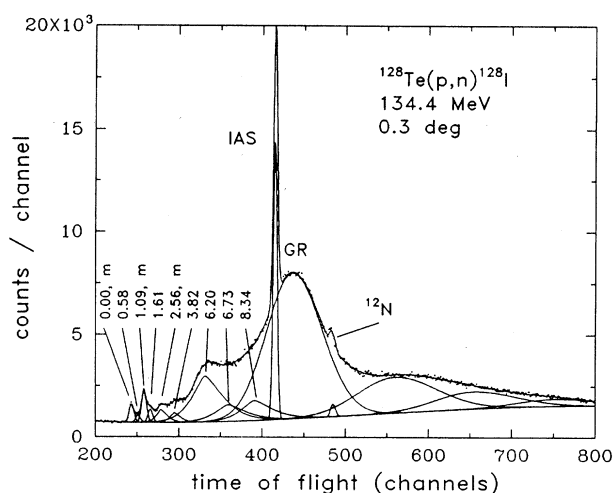


FIG. 7. Neutron time-of-flight spectrum at 0.3 deg from the $^{128}\text{Te}(p,n)^{128}\text{I}$ reaction at 134.4 MeV. The solid lines show the results using the code ALLFIT to fit the peaks simultaneously above the polynomial background.

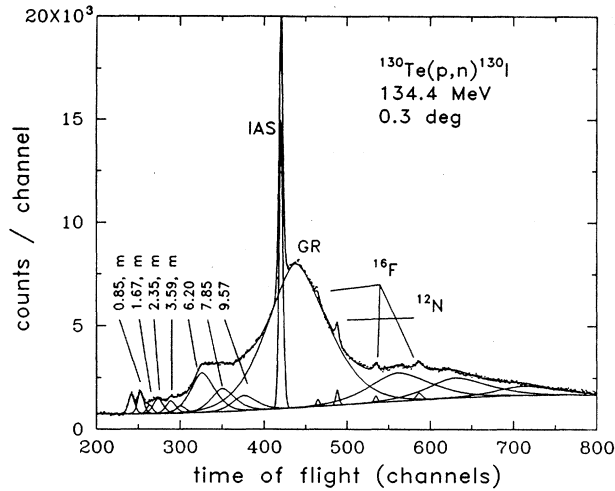


FIG. 8. Neutron time-of-flight spectrum at 0.3 deg from the $^{130}\text{Te}(p,n)^{130}\text{I}$ reaction of 134.4 MeV. The solid lines show the results using the code ALLFIT to fit the peaks simultaneously above the polynomial background.

integration, calculated neutron-detection efficiencies, and measured solid angle. The uncertainty in the target thickness is given in Table I. The beam charge was measured with a well-shielded split Faraday cup located approximately 10 m downstream from the target, and is estimated to be accurate to $\pm 5\%$. The uncertainty in the calculated detection efficiency is estimated to be about 11%, which is a quadrature sum of about 5% from the Monte Carlo code and about 9% from threshold uncertainties. The uncertainty in the solid angle of less than 0.5% is due largely to the ± 0.2 m uncertainty in the mea-

sured flight path. The differential cross sections were corrected for the attenuation of the neutron flux in transit from the target to the detectors and for the computer dead time. The calculation of the attenuation introduces an uncertainty in the cross sections of less than $\pm 5\%$. The systematic uncertainty estimated from all of these sources is $\pm 13\%$; however, for the $^{82}\text{Se}(p,n)^{82}\text{Br}$ reaction, the systematic uncertainty is probably 50–60% because of a crescent-shaped crack in the target. This estimate of the systematic uncertainty was obtained by requiring that the cross sections for the isobaric-analog states are proportional to $(N-Z)$ after accounting for differences in the distortion factors; accordingly, we expect the ratio of the IAS cross sections for ^{76}Ge and ^{82}Se to be

$$\frac{\sigma_{76}(\text{IAS})}{\sigma_{82}(\text{IAS})} = \frac{(N-Z)_{76}}{(N-Z)_{82}} \cdot \frac{N_D^{76}}{N_D^{82}} = \frac{12 (0.247)}{14 (0.240)} = 0.88 .$$

The distortion factors N_D were obtained from the ratio of a DWIA calculation to a plane-wave impulse approximation (PWIA) calculation. From the IAS cross sections at 0.3 deg reported in Tables III and IV, we have

$$\frac{\sigma_{76}(\text{IAS})}{\sigma_{82}(\text{IAS})} = \frac{7.76}{5.70} = 1.36 .$$

Thus, for this ratio to be equal to 0.88, $\sigma_{82}(\text{IAS})$ would need to be increased to 8.82 mb/sr, or by about 55%. Statistical uncertainties, listed in Tables III–VI, are typically less than 3%. The total uncertainty in the relative areas of the peaks could be significantly greater, especially for broad peaks, or in cases where there is no evident peak in the spectrum but strength is required to reproduce the overall spectral shape (e.g., the peak at 8.06 MeV in ^{76}As). These peaks are denoted with an asterisk in Tables III–VI.

TABLE III. The angular distribution of the differential cross sections for the peaks observed in the spectrum at 0.3 deg and the associated reduced transition probabilities $B(\text{GT})$ for the $\Delta L=0, 1^+$ transitions observed with the $^{76}\text{Ge}(p,n)^{76}\text{As}$ reaction at 134.4 MeV. An asterisk denotes a broad peak required to reproduce the overall shape.

Excitation energy E_x (MeV)	J^π	Center-of-mass cross section (mb/sr)						$\sigma_{\text{GT}}(q_{\text{min}})$ $q_{\text{min}}=0.016 \text{ fm}^{-1}$	Reduced transition probability $B(\text{GT})$
		0.3 deg $\sigma \pm \Delta\sigma$		4.0 deg $\sigma \pm \Delta\sigma$		8.5 deg $\sigma \pm \Delta\sigma$			
0.05	mixed	0.71	0.02	0.55	0.02	0.50	0.03	0.68	0.15
0.99	1^+	1.39	0.02	0.86	0.02	0.51	0.03	1.40	0.32
1.72	mixed	0.78	0.02	0.47	0.02	0.38	0.03	0.79	0.18
2.65	1^+	1.88	0.02	1.33	0.05	0.62	0.04	1.91	0.44
3.68	1^+	1.85	0.06	1.28	0.06	0.38	0.04	1.90	0.43
*5.48	1^+	13.85	0.17	8.20	0.20	3.28	0.32	14.56	3.36
*8.06	1^+	10.04	0.22	5.71	0.25	2.58	0.23	11.05	2.58
8.24(IAS)	0^+	7.76	0.06	5.11	0.05	1.37	0.04	(8.57)	
11.13(GR)	1^+	44.49	0.34	30.19	0.51	6.88	0.47	52.64	12.43
									19.89
*16.60		10.90	0.20	13.00	0.31	10.39	0.66		
*20.33		9.14	0.17	14.69	0.22	16.90	0.43		
*24.81		5.49	0.13	6.52	0.16	3.54	0.36		

TABLE IV. The angular distribution of the differential cross sections for the peaks observed in the spectrum at 0.3 deg and the associated reduced probabilities $B(\text{GT})$ for the $\Delta L=0, 1^\pm$ transitions observed with the $^{82}\text{Se}(p, n)^{82}\text{Br}$ reaction at 134.4 MeV. An asterisk denotes a broad peak required to reproduce the overall shape.

Excitation energy E_x (MeV)	J^π	^a Center-of-mass cross section (mb/sr)						$\sigma_{\text{GT}}(q_{\text{min}})$ $q_{\text{min}}=0.009 \text{ fm}^{-1}$	Reduced transition probability
		0.3 deg $\sigma \pm \Delta\sigma$		4.0 deg $\sigma \pm \Delta\sigma$		8.5 deg $\sigma \pm \Delta\sigma$			
0.08	mixed	0.97	0.12	0.85	0.02	0.37	0.02	0.97	0.34
1.50	$\Delta L \neq 0$	0.16	0.01	0.16	0.01	0.25	0.02		
2.14	mixed	0.65	0.01	0.58	0.02	0.25	0.01	0.66	0.23
2.7	$\Delta L \neq 0$	0.25	0.01	0.24	0.04	0.56	0.02		
3.10	mixed	0.40	0.02	0.33	0.04	0.36	0.02	0.38	0.13
3.47	mixed	0.43	0.02	0.40	0.04	0.31	0.02	0.42	0.14
4.19	1^+	2.30	0.03	2.01	0.08	0.73	0.03	2.37	0.84
5.43	1^+	4.27	0.07	3.37	0.18	1.07	0.04	4.46	1.58
*6.95	1^+	4.45	0.09	3.96	0.21	1.79	0.06	4.77	1.70
*8.77	1^+	4.47	0.11	3.63	0.16	1.29	0.08	4.97	1.79
9.58	0^+	5.70	0.04	4.76	0.05	1.24	0.03	(6.46)	
12.00	1^+	34.29	0.18	29.63	0.31	6.88	0.11	41.54	15.16
									21.91
*17.54		6.88	0.13	11.52	0.24	9.32	0.27		
*21.09		5.82	0.11	12.67	0.20	16.31	0.35		
*25.04		3.93	0.09	6.29	0.15	4.42	0.26		

^aBecause of the crack in the ^{82}Se target, these cross sections are probably too small by about 50–60%. Because $B(\text{GT})$ is determined by the ratio to the IAS strength, values of $B(\text{GT})$ are not affected by this effect.

V. GAMOW-TELLER STRENGTH

The total GT strength observed in each of these four (p, n) reactions was extracted by normalizing the GT strength in the 1^+ peaks to the Fermi transition strength $B(F)$ which is concentrated in the 0^+ IAS transition and

has the value $B(F) = N - Z$. Thus, our results for GT strengths are independent of normalization uncertainties such as those encountered for ^{82}Se . The sum rule for allowed transition strength relates the neutron excess of a target nucleus to the difference in the strength of β^- and β^+ transitions:^{1,2}

TABLE V. The angular distribution of the differential cross sections for the peaks observed in the spectrum at 0.3 deg and the associated reduced transition probabilities $B(\text{GT})$ for the $\Delta L=0, 1^+$ transitions observed with the $^{128}\text{Te}(p, n)^{128}\text{I}$ reaction at 134.4 MeV. An asterisk denotes a broad peak required to reproduce the overall shape.

Excitation energy E_x (MeV)	J^π	Center-of-mass cross section (mb/sr)						$\sigma_{\text{GT}}(q_{\text{min}})$ $q_{\text{min}}=0.021 \text{ fm}^{-1}$	Reduced transition probability $B(\text{GT})$
		0.3 deg $\sigma \pm \Delta\sigma$		4.0 deg $\sigma \pm \Delta\sigma$		8.5 deg $\sigma \pm \Delta\sigma$			
0.00	mixed	0.50	0.02	0.38	0.02	0.34	0.02	0.48	0.17
0.58	1^+	0.15	0.02	0.13	0.04	0.07	0.03	0.15	0.05
1.09	mixed	0.89	0.02	0.73	0.02	0.56	0.04	0.85	0.30
1.61	1^+	0.32	0.09	0.18	0.02	0.14	0.03	0.32	0.12
*2.56	mixed	1.15	0.05	0.58	0.04	2.46	0.75	1.18	0.43
3.82	1^+	1.01	0.06	0.39	0.04	0.36	0.04	1.05	0.38
*6.20	1^+	6.52	0.81	4.51	0.80	2.17	0.61	7.15	2.62
*6.73	1^+	1.42	0.73	1.16	0.32	0.48	0.11	1.58	0.58
*8.34	1^+	2.77	0.35	1.65	0.17	0.97	0.17	3.22	1.19
11.88 (IAS)	0^+	8.05	0.05	4.96	0.06	1.96	0.04	(10.65)	
13.14 (GR)	1^+	64.88	0.38	41.84	0.59	26.44	2.41	90.65	34.24
									40.08
*21.60		15.25	0.17	20.77	0.36	25.42	2.78		
*26.71		6.51	0.14	12.40	0.41	9.62	0.96		

TABLE VI. The angular distribution of the differential cross sections for the peaks observed in the spectrum at 0.3 deg and the associated reduced transition probabilities $B(\text{GT})$ for the $\Delta L=0, 1^\pm$ transitions observed with the $^{130}\text{Te}(p,n)^{130}\text{I}$ reaction at 134.4 MeV. The asterisk denotes the broad peak or peak required to reproduce overall shape.

Excitation energy E_x (MeV)	J^π	Center-of-mass cross section (mb/sr)						$\sigma_{\text{GT}}(q_{\text{min}})$ $q_{\text{min}}=0.013 \text{ fm}^{-1}$	Reduced transition probability $B(\text{GT})$
		0.3 deg $\sigma \pm \Delta\sigma$		4.0 deg $\sigma \pm \Delta\sigma$		8.5 deg $\sigma \pm \Delta\sigma$			
0.08	2^-	0.84	0.02	1.12	0.04	1.11	0.04		
0.85	mixed	0.89	0.04	0.58	0.03	0.67	0.04	0.85	0.32
*1.67	mixed	0.34	0.03	0.22	0.03	0.30	0.04	0.32	0.12
*2.35	mixed	1.40	0.06	0.63	0.05	0.77	0.09	1.38	0.52
*3.59	mixed	0.78	0.06	0.35	0.06	0.46	0.08	0.80	0.29
*4.20	$\Delta L \neq 0$	0.43	0.04	0.45	0.08	0.24	0.06		
*6.20	1^+	7.85	0.37	5.84	0.55	4.35	0.71	8.49	3.25
*7.85	1^+	3.86	0.26	2.30	0.31	2.05	0.37	4.34	1.68
*9.57	1^+	2.74	0.22	1.66	0.18	1.52	0.21	3.24	1.26
12.48 (IAS)	0^+	8.35	0.06	4.27	0.09	1.08	0.04	(11.00)	
13.59 (GR)	1^+	70.30	0.56	56.67	1.60	23.74	1.92	97.18	38.46
									45.90
*21.05		14.68	0.27	18.65	0.75	24.19	2.18		
*24.79		11.18	0.27	14.85	0.86	13.44	1.83		
*29.11		5.73	0.19	6.03	0.40	6.96	0.84		

$$S_{\beta^-}(\text{GT}) - S_{\beta^+}(\text{GT}) = 3(N - Z). \quad (1)$$

The strength $S_{\beta^\pm}(\text{GT})$ is given by the sum of the reduced transition probabilities $B(\text{GT}^\pm)$ for all β^\pm transitions from the ground state of the target nucleus to all possible final states in the residual nucleus; that is,

$$S_{\beta^\pm}(\text{GT}) = \sum_f B(\text{GT}; i \rightarrow f)^{\beta^\pm}, \quad (2)$$

$$B(\text{GT}; i \rightarrow f)^{\beta^\pm} = \langle M(\text{GT}) \rangle^2 = \left| \langle f | \sum_{k=1} \sigma_k \cdot \tau_k^\pm | i \rangle \right|^2. \quad (3)$$

The reduced transition probabilities are defined such that $B(F)=1$ and $B(\text{GT})=3$ for the beta decay of the free neutron. These sum rules are independent of the structure of the nuclei involved except that they are assumed to contain neutrons and protons and not, for example, π mesons or Δ resonances.

At low momentum transfers, the noncentral parts of the effective interaction become small; therefore, in the distorted-wave impulse-approximation, the (p,n) cross section at the minimum kinematically allowed momentum transfer q_{min} can be written

$$\sigma_F(q=q_{\text{min}}) \sim N_D(F) (k_f/k_i) B(F) |V_\tau|^2, \quad (4)$$

and

$$\sigma_{\text{GT}}(q=q_{\text{min}}) \sim N_D(\text{GT}) (k_f/k_i) B(\text{GT}) |V_{\sigma\tau}|^2. \quad (5)$$

Here the N_D 's are distortion factors produced from the integration of the distorted waves; $|V_\tau|^2$ and $|V_{\sigma\tau}|^2$ are volume integrals of the effective interactions $V_\tau(r)(\tau_1\tau_2)$

and $V_{\sigma\tau}(r)(\sigma_1\sigma_2)(\tau_1\tau_2)$, respectively, and k_i and k_f are the wave numbers of the incident proton and the outgoing neutron. The ratio of these two cross sections is

$$\frac{\sigma_{\text{GT}}(q=q_{\text{min}})}{\sigma_F(q=q_{\text{min}})} = \frac{B(\text{GT})}{B(F)} \frac{k_f^{\text{GT}}}{k_f^F} \frac{N_D(\text{GT})}{N_D(F)} \frac{|V_{\sigma\tau}|^2}{|V_\tau|^2}. \quad (6)$$

From comparisons of (p,n) reactions with associated beta-decay transitions, Taddeucci *et al.*^{22,23} determined the following relationship:

$$D = \frac{N_D(\text{GT})}{N_D(F)} \frac{|V_{\sigma\tau}|^2}{|V_\tau|^2} \sim - \left[\frac{E_p}{55.0 \pm 0.4} \right]^2. \quad (7)$$

From Eqs. (6) and (7), the relationship between $B(\text{GT})$ and $\sigma_{\text{GT}}(q=q_{\text{min}})$ is

$$B(\text{GT}) = \frac{\sigma_{\text{GT}}(q=q_{\text{min}})}{\sigma_F(q=q_{\text{min}})} \frac{B(F)}{D} \frac{k_f^F}{k_f^{\text{GT}}}. \quad (8)$$

For the measurements reported here, $E_p=134.4$ MeV; thus, from Eq. (7), the ratio $D=6.0$. Because the momentum transfer depends on the excitation energy of the residual nucleus, it is necessary that the cross section extracted for each peak at 0.3 deg be extrapolated to the kinematic-minimum-momentum transfer. This extrapolation is performed for each reaction with a shape calculated in the DWIA for an average of several, $\Delta L=0, 1^+$ transitions with 1p-1h harmonic-oscillator wave functions. The momentum-transfer dependence of the normalized cross section for each of these average $\Delta L=0$ shapes is shown in Fig. 9. The effective interaction of Franey and Love¹⁸ at 140 MeV was used for these DWIA calculations. The momentum transfers for the GTGR

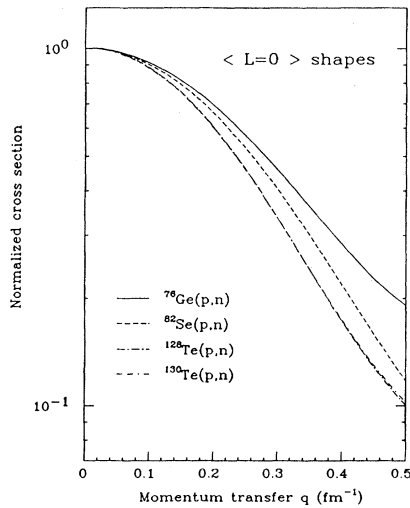


FIG. 9. The momentum-transfer dependence of the normalized cross section calculated in the DWIA for an average of several $\Delta L=0$, 1^+ transitions for (p,n) reactions on ^{76}Ge , ^{82}Se , ^{128}Te , and ^{130}Te .

transitions are 0.135, 0.135, and 0.162, and 0.157 fm^{-1} for (p,n) reactions on ^{76}Ge , ^{82}Se , ^{128}Te , and ^{130}Te , respectively. In the region of interest (below 0.2 fm^{-1}), the DWIA calculations for individual transitions with the 1p-1h wave functions show only small ($< 8\%$) deviations from the average curve for all the transitions. The average $\Delta L=0$ shape calculated for the $^{76}\text{Ge}(p,n)^{76}\text{As}$ reaction with the wave functions in Table IX differed only slightly from that plotted in Fig. 9 for 1p-1h wave functions. The average shapes agree well with the distributions measured for the GTGR transitions.

The ratio k_f^F/k_f^{GTGR} is slightly larger than one because the centroid of the observed GT strength is at a slightly higher-excitation energy than that of the IAS. Values of the ratio k_f^F/k_f^{GTGR} are 1.012, 1.010, 1.005, and 1.005 for ^{76}As , ^{82}Br , ^{128}I , and ^{130}I , respectively.

The center-of-mass cross section of the peaks extracted at 0.3 deg above the polynomial background and the associated $B(\text{GT})$ values from Eq. (8) for the $\Delta L=0$, 1^+ transitions are listed in Tables III–VI, respectively, for the (p,n) reactions on ^{76}Ge , ^{82}Se , ^{128}Te , and ^{130}Te , respectively. The cross sections $\sigma_{\text{GT}}(q=q_{\text{min}})$ in the sixth column of each of these tables are the values extrapolated to the smallest kinematically allowed momentum transfer q_{min} . The resulting β^- strength $S_{\beta^-}(\text{GT})$ is 19.9, 21.9, 40.1, and 45.9 in ^{76}As , ^{82}Br , ^{128}I , and ^{130}I , respectively; and the respective percentages of the $3(N-Z)$ sum rule extracted in this way are 55, 52, 56, and 59 if the β^+ strength $S_{\beta^+}(\text{GT})$ is assumed to be zero. The portion of this GT strength in low-lying 1^+ transitions (denoted LL in Table VIII) is 25, 23, 15, and 17%, respectively, for ^{76}As , ^{82}Br , ^{128}I , and ^{130}I . The $B(\text{GT})$ distributions are given in the form of bar graphs in panels (b) of Figs. 1–4.

An upper limit on the GT strength contained in the subtracted background under the GTGR was obtained by assigning the strength above the cosmic-ray and overlap

backgrounds to $\Delta L=0$, GT transition strength. The cross-section strength observed at 0.3 deg was binned into 2-MeV wide bins and interpolated to q_{min} . These cross sections were converted to $B(\text{GT})$ with Eq. (8) and summed from 0-MeV excitation to the high-excitation side of the GTGR. The sum from 0 to 16 MeV is 3.4 for ^{76}As and 3.1 for ^{82}Br ; the sum from 0 to 18 MeV is 11.4 for ^{128}I and 9.5 for ^{130}I . These values are upper limits to the GT strength because no attempt was made to subtract $\Delta L \neq 0$ components from the 0.3 deg cross sections. The total GT strength, consisting of the sum of the strength observed in the peaks plus the estimated contribution from the background, is 23.3, 24.6, 51.5, and 55.4 for ^{75}As , ^{82}Br , and $^{128,130}\text{I}$, respectively, which correspond to 65, 59, 72, and 71% of the $3(N-Z)$ sum rule.

VI. COMPARISON WITH CALCULATIONS OF THE GAMOW-TELLER STRENGTH FUNCTIONS

The Gamow-Teller strength function can be calculated with a variety of nuclear models which include extensions of the simple 1p-1h shell model. The calculations presented here are based on the model of Grotz, Klapdor, and Metzinger,²⁴ which includes ground-state (g.s.) correlations in the target nucleus. This model includes deviations from simple shell-model ground-state configurations by approximating the distribution of nucleons around the Fermi levels with occupation amplitudes calculated by means of the Bardeen-Cooper-Schrieffer (BCS) theory of superfluid-pairing correlations of nucleons.²⁵ In an earlier work,²⁶ it was demonstrated that the GT strength distribution in ^{208}Bi is sensitive to small occupations of high-lying neutron orbits and small vacancies in proton orbits. Pairing correlations lead to a coherent contribution of many shells to the transition matrix elements. The 1^+ states in the residual nucleus are calculated in the Tamm-Dancoff approximation which confines the calculation to 1p-1h configurations. The wave functions of the 1^+ states in the residual nucleus are obtained by diagonalizing a Hamiltonian with a long-range residual neutron-proton interaction in the spin-isospin channel of the form

$$H_{\sigma\tau} = 2\chi \sum_{i,j=1}^A \sigma(i)\sigma(j) [\tau^+(i)\tau^-(j) + \tau^-(i)\tau^+(j)], \quad (9)$$

where $\sigma(i)$ is the Pauli spin operator and $\tau^\pm(i)$ are isospin raising and lowering operators acting on the i th nucleon. The coupling constant χ is adjusted to reproduce the known excitation energy of the GTGR with the result that the value of the product $A\chi$, where A is the mass number of the target, is 14.8, 15.5, 20.1, and 20.4 MeV for ^{76}Ge , ^{82}Se , ^{128}Te , and ^{130}Te , respectively. Also the effect of correlations arising from this long-range force in the ground states of the parent nuclei was included. A residual interaction of this type can account for the collective features of GT transitions. This spin-isospin force is responsible not only for concentrating the 1^+ strength from (p,n) reactions on 0^+ targets into the GTGR, but also for reducing or quenching the total β^+ strength (and

to a lesser degree the β^- strength) by ground-state correlations. For the calculation presented here, the Hamiltonian is

$$H = H_{\text{sp}} + H_{\text{pair}} + H_{\sigma\tau}. \quad (10)$$

Here $H_{\sigma\tau}$ is given by Eq. (9); and the Hamiltonian H_{sp} , which specifies the energies of the single-particle levels, is obtained from a Nilsson potential (with zero deformation) for a spherical nucleus. The single-particle energies in units of $\hbar\omega$ are listed in Table VII(top) for ^{76}Ge , and ^{82}Se , and in Table VII(bottom) for ^{128}Te and ^{130}Te . The oscillator energy $\hbar\omega = 41 \text{ MeV}/A^{1/3}$; values are 9.68, 9.44, 8.14, and 8.09 MeV, respectively, for ^{76}Ge , ^{82}Se , ^{128}Te , and ^{130}Te . The single-particle energies used in the calculations were modified slightly for the tellurium isotopes to obtain better agreement with quasiparticle states in the nuclei of $^{127,129}\text{Sn}$, ^{135}Cs , and ^{139}La .

For the pairing forces, the Hamiltonian is

$$H_{\text{pair}} = -G_n \sum_{kk'} a_{kn}^\dagger a_{kn}^\dagger a_{k'n} a_{k'n} - G_p \sum_{kk'} a_{kp}^\dagger a_{kp}^\dagger a_{k'p} a_{k'p}. \quad (11)$$

Here G_n (G_p) is the strength of the neutron-neutron (proton-proton) interaction. The neutron-proton pairing

TABLE VII. Single-particle energies in units of $\hbar\omega$ ($=41 \text{ MeV}/A^{1/3}$).

Shell	^{76}Ge and ^{82}Se	
	Neutrons	Protons
$1d_{5/2}$	3.22	3.32
$1d_{3/2}$	3.67	3.68
$2s_{1/2}$	3.69	3.70
$1f_{7/2}$	4.18	4.17
$1f_{5/2}$	4.67	4.67
$2p_{3/2}$	4.69	4.70
$2p_{1/2}$	4.90	4.92
$1g_{9/2}$	5.00	4.97
$1g_{7/2}$	5.63	5.63
$2d_{5/2}$	5.66	5.67
$2d_{3/2}$	6.01	6.03
$3s_{1/2}$	6.02	6.05
Shell	^{128}Te and ^{130}Te	
	Neutrons	Protons
$1f_{5/2}$	4.67	4.65
$2p_{3/2}$	4.65	4.70
$2p_{1/2}$	4.85	4.90
$1g_{9/2}$	5.10	5.00
$2d_{5/2}$	5.55	5.67
$1g_{7/2}$	5.67	5.58
$1h_{11/2}$	5.83	5.78
$2d_{3/2}$	5.86	6.01
$3s_{1/2}$	5.76	6.04
$2f_{1/2}$	6.55	6.61
$1h_{9/2}$	6.58	6.52
$1h_{13/2}$	6.94	6.90
$1f_{5/2}$	7.01	7.08

interaction is small and can be neglected. The operators a_k^\dagger and $a_{\bar{k}}^\dagger$ are nucleon creation operators, and $a_{k'}$ and $a_{\bar{k}'}$ are nucleon destruction operators. The bar denotes the time-conjugated state. The sum over k and k' includes the quantum numbers of the particles and holes in the initial and final states. The strengths of the pairing interactions are taken to be $G_n(\text{MeV}) = 22/A$ and $G_p(\text{MeV}) = 24.5/A$.

Diagonalization of the dominant part of the Hamiltonian H , namely $H_{\text{sp}} + H_{\text{pair}}$, in terms of the BCS formalism gives the energies E_{qp} of unperturbed quasiparticle (QP) states. Diagonalization of the total Hamiltonian

$$H = E_{qp} \alpha_{qp}^\dagger \alpha_{qp} + h_{\sigma\tau}$$

in the space of two-quasiparticle (2QP) states yields the 1^+ states in the residual nucleus. The ground state of the target nucleus follows from diagonalization of 4QP configurations. The $B(\text{GT})$ values are obtained from the matrix elements of the GT operator between the 0^+ ground state of the target nucleus and the 1^+ states in the residual nucleus. The calculations were performed in a basis large enough to include allowed transitions with unperturbed strength down to about 1% of that for a single-particle value transition.

The $B(\text{GT})$ distribution obtained from the shell-model calculations are shown in panels (c) of Figs. 1–4. Listed in Table VIII for the four nuclei studied here are the measured and the calculated values of (1) the sum of the low-lying GT strength, (2) the strength in the GTGR region, (3) the total GT strength above the background, and (4) the ratios of the measured to the calculated values of the GT strengths in (1), (2), and (3). The ratios in Table VIII are a measure of the quenching of the GT strength in the low-lying region, in the region of the GTGR, and in the total observed excitation-energy region. A striking feature of this comparison is that the low-lying strength apparently is not quenched relative to the calculated strength, at least for the model employed

TABLE VIII. Measured and calculated values of the total GT strength in the peaks above the background, the strength in the GTGR region, the sum of the low-lying GT strength, and the ratios of the measured to the calculated values of the GT strength in ^{76}As , ^{82}Br , ^{128}I , and ^{130}I .

Target	Region ^a	$B_{\text{expt}}(\text{GT})$	$B_{\text{th}}(\text{GT})$	$B_{\text{expt}}(\text{GT})/B_{\text{th}}(\text{GT})$
^{76}Ge	LL (< 6 MeV)	4.9	3.2	1.53
	GTGR	12.4	34.4	0.36
	Total (< 25 MeV)	19.9	37.6	0.53
^{82}Se	LL (< 7 MeV)	5.0	3.8	1.32
	GTGR	15.2	38.8	0.39
	Total (< 25 MeV)	21.9	42.5	0.52
^{128}Te	LL (< 10 MeV)	5.8	7.4	0.79
	GTGR	34.2	63.8	0.54
	Total (< 25 MeV)	40.1	71.1	0.56
^{130}Te	LL (< 10 MeV)	7.4	7.3	1.01
	GTGR	38.5	69.7	0.55
	Total (< 25 MeV)	45.9	76.9	0.60

^aLL denotes low-lying strength below the GTGR.

here; in contrast, the total GT strength is quenched by about 40% for ^{130}Te to 49% for ^{82}Se ; and the strength in the GTGR, by about 45% for ^{130}Te to 64% for ^{76}Ge . This excitation-energy dependence of the quenching was predicted by Grotz *et al.*²⁴ as a result of including $\Delta - N^{-1}$ admixtures into the ground state of the target nucleus. A perturbative treatment of the mixing process produces a destructive interference of the first- and second-order contributions for the transitions at low-excitation energies. It should be noted that configuration mixing with multiparticle-multihole states in the continuum also causes more "quenching" in the GTGR than in the low-lying states.

About half of the calculated low-lying strength is concentrated in a collective state at 5-MeV excitation energy in the ^{78}As and ^{82}Br isotopes and around 7 MeV in the Te isotopes, whereas the first three low-lying states in each case are nearly pure particle-hole configurations; as an example, we show in Table IX the wave functions of the low-lying 1^+ states, and the main contributions to the GTGR in ^{76}As . The lowest 1^+ state, which we identify with the ground state in the cases of ^{82}Br and ^{128}I , is a "back-spin-flip" configuration with a quasiparticle representation $\nu 2p^{1/2} - \pi 2p^{3/2}$ for ^{76}As and ^{82}Br and $\nu 2d_{3/2} - \pi 2d_{5/2}$ for the Te isotopes. "Back-spin-flip" transitions of the type

$$\nu(j = l - \frac{1}{2}) \rightarrow \pi(j = l + \frac{1}{2})$$

occur only in nuclei with a large neutron excess and are responsible for the lowest-lying GT strength in neutron-rich nuclei.²⁷

VII. DIFFERENCE IN GT STRENGTHS FROM ^{128}Te AND ^{130}Te

Our results for the Te isotopes are of particular interest because one can obtain information about the $\beta\beta$ -decay process from the measured ratio of half-lives of the two isotopes, provided that the $\beta\beta$ -decay matrix elements for the two neighboring isotopes are the same.^{5,6,28} Because the decay energies T_0 for ^{128}Te and ^{130}Te differ greatly (869 and 2533 keV, respectively) and the dependence of the $\beta\beta$ -decay rate on T_0 is much stronger for 2ν decay than for 0ν decay, the half-life ratio $R = \tau(128)/\tau(130)$ depends on the relative importance of 2ν and 0ν decay. Qualitatively, if the matrix elements are equal, then $R_{2\nu} = 5130$ and $R_{0\nu} = 25$, while a lower limit on the experimental value of R is about 2000;^{29,30} thus, provided that the matrix elements are indeed equal, experimental observations do not rule out contributions to Te decay from both 2ν and 0ν processes. Recent calculations^{31,32} of 2ν decay of $^{128,130}\text{Te}$ are consistent with 100% 2ν decay of both nuclides.

Our present results can shed some light on the other assumption involved in this analysis; the equality of the matrix elements. The neutron spectra from $^{128,130}\text{Te}$ were obtained with an energy resolution of about 340 keV. The polynomial background, which was used to fit each TOF spectrum as described in Sec. III, was subtracted from each spectrum. Then a difference spectrum was obtained by normalizing the spectra so that the yield of the IAS is proportional to $N - Z$; this procedure should eliminate many systematic uncertainties. The state at $E_x = 80$ keV in ^{130}I was deleted from the spectrum because this state was found to have an angular distribution with

TABLE IX. Wave functions and transition strengths for the low-lying 1^+ states and the three main contributions to the GTGR in ^{76}As .

Configuration		Excitation energy (MeV)									
<i>n</i>	<i>p</i>	0.22	1.22	2.03	2.77	4.04	4.57	5.12	9.96	11.52	12.26
$2p_{1/2}$	$2p_{3/2}$	-0.98	-0.14	0.09	0.00	0.03	0.03	0.06	-0.06	0.04	-0.06
$1f_{5/2}$	$1f_{5/2}$	0.17	-0.97	0.08	-0.07	0.03	0.04	0.09	-0.10	0.04	-0.07
$2p_{3/2}$	$2p_{3/2}$	-0.02	-0.12	-0.06	0.95	-0.14	-0.02	-0.14	0.12	-0.07	0.11
$1f_{5/2}$	$1f_{7/2}$	0.05	0.08	-0.04	0.07	-0.28	0.82	0.47	-0.07	0.04	-0.06
$2p_{1/2}$	$2p_{1/2}$	0.09	0.10	0.99	0.09	0.01	-0.01	0.05	-0.03	0.02	-0.03
$1g_{9/2}$	$1g_{9/2}$	-0.06	-0.09	0.08	-0.25	-0.82	0.02	-0.41	0.20	-0.09	0.15
$2p_{3/2}$	$2p_{1/2}$	-0.03	-0.05	0.06	-0.07	0.45	0.56	-0.63	0.18	-0.10	0.15
$1f_{7/2}$	$1f_{5/2}$	-0.03	-0.05	0.03	-0.07	0.12	-0.09	0.28	0.42	-0.19	0.27
$1g_{7/2}$	$1g_{9/2}$	0.02	0.02	-0.01	0.02	-0.01	-0.04	-0.13	-0.08	0.07	-0.08
$1g_{9/2}$	$1g_{7/2}$	-0.04	-0.04	0.03	-0.07	0.08	-0.02	0.30	0.52	-0.25	0.33
$1f_{7/2}$	$1f_{7/2}$	-0.02	0.03	0.00	-0.01	0.02	-0.02	0.02	-0.46	-0.22	0.21
$2d_{5/2}$	$2d_{5/2}$	-0.01	-0.01	0.00	-0.01	0.01	0.00	0.03	-0.38	-0.62	0.19
$1g_{7/2}$	$1g_{7/2}$	0.01	0.01	-0.01	0.02	0.05	0.00	0.02	0.15	0.36	0.20
$2d_{5/2}$	$2d_{3/2}$	-0.01	-0.01	0.00	-0.01	0.01	0.00	0.03	-0.23	0.54	0.78
$2d_{3/2}$	$2d_{5/2}$	0.00	0.00	0.00	0.00	0.00	0.00	-0.01	0.08	-0.08	-0.03
$3s_{1/2}$	$3s_{1/2}$	0.00	0.00	0.00	0.00	0.00	0.00	0.01	-0.04	0.05	-0.12
$2d_{3/2}$	$2d_{3/2}$	0.00	0.00	0.00	0.00	0.00	0.00	-0.01	0.05	0.12	0.04
B_{GT}		0.19	0.24	0.11	0.37	0.49	0.10	1.72	10.82	5.48	13.91

$\Delta L > 0$; therefore, it does not contribute to the $\beta\beta$ process. For the mixed transitions (see Tables V and VI), the $L=0$ strength dominates at 0 deg, so these states are left in the spectra. Also, before obtaining the difference spectrum, the strength was deleted from transitions to states in ^{16}F and ^{12}C . The resulting difference spectrum is plotted in Fig. 10 as the fractional difference $1 - Y(^{128}\text{Te})/Y(^{130}\text{Te})$ in the normalized yields of the allowed ($\Delta L=0$) GT strength versus the neutron time of flight. An excitation energy scale is shown as an inset; the reference energy is the energy of the IAS. The fractional difference is small in the neighborhood of the GTGR, but differs by larger amounts at low-excitation energy where the GT strength is small and measured with greater statistical uncertainty. Averaged over the entire excitation energy spectrum, the difference is about 3% favoring ^{130}Te ; however, it increases to about 7% when the transitions are weighted by the reciprocal of the energy. The energy denominator in the transition amplitude emphasizes the low-lying transitions.^{5,6} For the excitation-energy region below the IAS, the energy-weighted fractional difference is about 15% also favoring ^{130}Te ; however, in this region the fractional difference decreases only slightly to about 14% if the transitions are not weighted by the reciprocal of the energy. We conclude that the matrix elements leading to the intermediate states in iodine do not differ significantly, and certainly not enough to invalidate the conclusion that both 2ν and 0ν processes might contribute to the decay process. Our results do not provide information about possible differences of matrix elements governing transitions from intermediate to final states. The matrix element for the second step of the $\beta\beta$ -decay process from the intermediate state to the final state can be compared to the reduced transition probability $B_{\text{GT}}^+(E)$, which could be extracted, in principle, from an (n,p) experiment with the daughter nucleus as the target; however, even with an (n,p) experiment for the second step, there still remains the experimentally inaccessible problem of determining the relative phase of the amplitudes for the two steps in $\beta\beta$ decay. (See the discussion in Ref. 31.) This problem may make the comparison of the GT strengths from ^{128}Te and ^{130}Te less constraining than it appears insofar as its effect on the $\beta\beta$ -decay rates is concerned; however, a combination of both (p,n) and (n,p) measurements and the assumption of purely constructive interference should yield an upper limit on the transition strength and a lower limit on the lifetime for the transition.

We conclude that the matrix elements leading to intermediate states in ^{128}I and ^{130}I do not differ much where

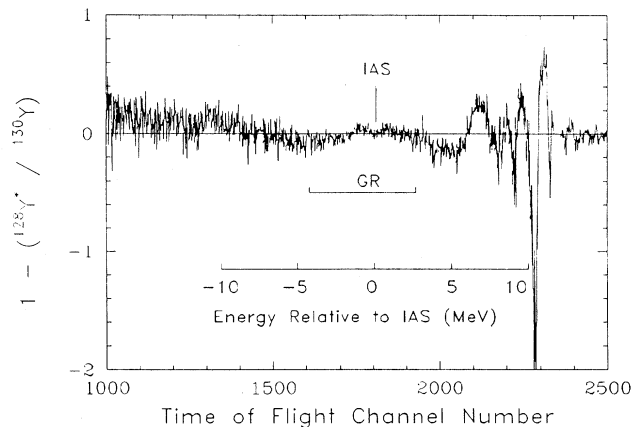


FIG. 10. Comparison of the yield of Gamow-Teller strength from the $^{128,130}\text{Te}(p,n)$ reactions at 134.4 MeV as a function of the neutron time of flight. The fractional difference $1 - Y^*(^{128}\text{Te})/Y(^{130}\text{Te})$ was obtained by subtracting a polynomial background from each spectrum and then normalizing the yield of the IAS in ^{128}Te to be proportional to $N - Z$.

the GT strength is large, although there are significant differences in the region of low-excitation energies. It is worth noting that theoretical calculations⁵ tend to support the equality of the ^{128}Te and ^{130}Te matrix elements.

VIII. CONCLUSIONS

The present experiment on targets of ^{76}Ge , ^{82}Se , ^{128}Te , and ^{130}Te together with that reported earlier²⁶ on ^{208}Pb has yielded the first detailed view of the low-lying structures excited by the (p,n) reaction in heavy nuclei. The GT strength observed in 1^+ transitions below the GTGR represents a significant portion of the total observed GT strength. Comparison of the observed GT strength with that obtained from a shell-model calculation shows that the low-lying strength is not quenched relative to the calculated strength. The significance of this result is that the quenching factor for the total strength should not be applied to calculations of low-lying transitions in heavy nuclei. The observation of the dependence of the quenching on excitation energy is consistent with a prediction of Grotz *et al.*²⁴ concerning the effect of the presence of Δ 's in the nucleus.

This research was supported in part by the National Science Foundation under Grant Nos. PHY 85-01054, PHY 88-02392, PHY 86-11210, and PHY 83-12245.

*Present address: University of Maryland, College Park, MD 20742.

¹K. I. Ikeda, S. Fujii, and J. I. Fujita, *Phys. Lett.* **3**, 271 (1963).

²C. Gaarde, J. S. Larsen, M. N. Harakeh, S. Y. van der Werf, M. Igarashi, and A. Müller-Arnke, *Nucl. Phys.* **A334**, 248 (1980).

³R. Madey, J. W. Watson, M. Ahmad, B. D. Anderson, A. R.

Baldwin, A. L. Casson, W. Casson, R. A. Cecil, A. Fazely, J. N. Knudson, C. Lebo, W. Pairsuwan, P. J. Pella, J. C. Varga, and T. R. Witten, *Nucl. Instrum. Methods* **214**, 401 (1983).

⁴B. S. Flanders, Ph.D. dissertation, Kent State University, 1985.

⁵W. C. Haxton and G. J. Stephenson, Jr., *Prog. Part. Nucl. Phys.* **12**, 490 (1984).

⁶M. Doi, T. Katani, and E. Takasugi, *Prog. Theor. Phys., Suppl.*

- No. **83**, 1 (1983).
- ⁷J. D. Vergados, *Phys. Rep.* **133**, 1 (1986); *Phys. Rev. C* **13**, 865 (1976).
- ⁸K. Grotz and H. V. Klapdor, *Nucl. Phys.* **A460**, 395 (1986).
- ⁹C. D. Goodman, C. C. Foster, M. B. Greenfield, C. A. Goulding, D. A. Lind, and J. Rapaport, *IEEE Trans. Nucl. Instrum. Methods* **171**, 149 (1980).
- ¹⁰A. R. Baldwin and R. Madey, *Nucl. Instrum. Methods* **171**, 149 (1980).
- ¹¹A. Fazely, M. Ahmad, B. D. Anderson, A. R. Baldwin, A. M. Kalenda, R. J. McCarthy, J. W. Watson, R. Madey, W. Bertozzi, T.N. Buti, J. M. Finn, M. A. Kovash, B. Pugh, and C. C. Foster, *Phys. Rev. C* **25**, 1760 (1982).
- ¹²R. A. Cecil, B. D. Anderson, and R. Madey, *Nucl. Instrum. Methods* **161**, 439 (1979).
- ¹³B. D. Anderson, J. N. Knudson, R. Madey, and C. C. Foster, *Nucl. Instrum. Methods* **169**, 135 (1980).
- ¹⁴J. W. Watson, B. D. Anderson, A. R. Baldwin, C. Lebo, B. S. Flanders, W. Pairsuwan, R. Madey, and C. C. Foster, *Nucl. Instrum. Methods* **215**, 413 (1983).
- ¹⁵J. D. Auria, M. Domskey, L. Moritz, T. Ruth, G. Sheffer, T. E. Ward, C. C. Foster, J. W. Watson, B. D. Anderson, J. Rapaport, *Phys. Rev. C* **30**, 1999 (1984).
- ¹⁶J. J. Kelly (unpublished).
- ¹⁷R. Schaeffer and J. Raynal, Program DWBA70 (unpublished); extended version, J. R. Comfort, DW81 (unpublished).
- ¹⁸M. A. Franey and W. G. Love, *Phys. Rev. C* **31**, 488 (1985).
- ¹⁹P. Schwandt, H. O. Meyer, W. W. Jacobs, A. D. Bacher, S. E. Vigdor, M. D. Kaitchuck, and T. R. Donoghue, *Phys. Rev. C* **26**, 55 (1982).
- ²⁰R. Madey, B. S. Flanders, B. D. Anderson, A. R. Baldwin, C. Lebo, J. W. Watson, Sam. M. Austin, A. Galonsky, B. H. Wildenthal, and C. C. Foster, *Phys. Rev. C* **35**, 2011 (1987).
- ²¹J. R. Wu, *Phys. Lett.* **91B**, 169 (1980).
- ²²T. N. Taddeucci, C. A. Goulding, T. A. Carey, R. C. Byrd, C. D. Goodman, C. Gaarde, J. Larsen, C. A. Goulding, D. J. Horen, T. Masterson, and E. Sugarbaker, *Nucl. Phys.* **A469**, 125 (1987).
- ²³T. N. Taddeucci, J. Rapaport, D. E. Bainum, C. D. Goodman, C. C. Foster, C. Gaarde, J. Larsen, C. A. Goulding, D. J. Horen, T. Masterson, and E. Sugarbaker, *Phys. Rev. C* **25**, 1094 (1981).
- ²⁴K. Grotz, H. V. Klapdor, and J. Metzinger, *Phys. Lett.* **132B**, 22 (1983).
- ²⁵V. G. Soloviev, *Theory of Complex Nuclei* (Pergamon, Oxford, 1976).
- ²⁶K. Grotz, H. V. Klapdor, J. Metzinger, R. Madey, W. Pairsuwan, B. D. Anderson, A. R. Baldwin, B. S. Flanders, C. Lebo, J. W. Watson, and C. C. Foster, *Phys. Lett.* **126B**, 417 (1983).
- ²⁷H. V. Klapdor, *Prog. Part. Nucl. Phys.* **10**, 137 (1983); **17**, 479 (1986).
- ²⁸B. Pontecorvo, *Phys. Lett.* **26B**, 630 (1968).
- ²⁹T. Kirsten, E. Heusser, D. Kaether, J. Oehm, E. Pernicka, and H. Richter, *Proceedings of the International Symposium on Nuclear Beta Decays and Neutrinos, Osaka, 1986* (World-Scientific, Singapore, 1986).
- ³⁰O. K. Manuel, *Proceedings of the International Symposium on Nuclear Beta Decays and Neutrinos, Osaka, 1986* (World-Scientific, Singapore, 1986).
- ³¹K. Muto and H. V. Klapdor, *Phys. Lett. B* **201**, 420 (1988).
- ³²K. Grotz and H. V. Klapdor, *Nucl. Phys.* **A460**, 395 (1986).